THE JOURNAL OF PHYSICAL CHEMISTRY B
A JOURNAL OF THE AMERICAN CHEMICAL SOCIETY

pubs.acs.org/JPCB

Article

Membrane Remodeling and Stimulation of Aggregation Following α-Synuclein Adsorption to Phosphotidylserine Vesicles

Published as part of The Journal of Physical Chemistry virtual special issue "Carol K. Hall Festschrift".

Brandon M. Hoover, Zhizhang Shen, Curran G. Gahan, David M. Lynn, Reid C. Van Lehn, and Regina M. Murphy*

Cite This: *J. Phys. Chem. B* 2021, 125, 1582−1594

Read Online

ACCESS | Metrics & More | Article Recommendations | Supporting Information

ABSTRACT: α-Synuclein is an intrinsically disordered protein abundant in presynaptic terminals in neurons and in synaptic vesicles. α-Synuclein's interaction with lipid bilayers is important not only for its normal physiological function but also in its pathological aggregation and deposition as Lewy bodies in Parkinson's disease. α-Synuclein binds preferentially to lipids with acidic head groups and to high-curvature vesicles and can modulate membrane curvature. The relationship between the protein's role as a membrane curvature sensor and generator and the role of membranes in facilitating its aggregation remains unknown. We investigated the interaction of α-synuclein with vesicles of 1,2-dioleoyl-*sn*-glycero-3-phospho-L-serine (DOPS) or 1,2-dilauroyl-*sn*-glycero-3-phospho-L-serine (DLPS). Using nanoparticle tracking along with electron microscopy, we demonstrate that α-synuclein induces extensive vesicle disruption and membrane remodeling into discoids, tubules, and ribbons with DLPS vesicles but not DOPS. Coarse-grained molecular dynamics simulations revealed that adsorption of α-synuclein to DLPS but not DOPS vesicles induced vesicle elongation and redistribution of protein to regions of higher curvature, a process that could drive protein aggregation. In agreement with this hypothesis, DLPS but not DOPS strongly stimulated α-synuclein aggregation. Our results provide new insights into the critical contribution of bilayer stability in the membrane response to α-synuclein adsorption and in stimulation of aggregation.

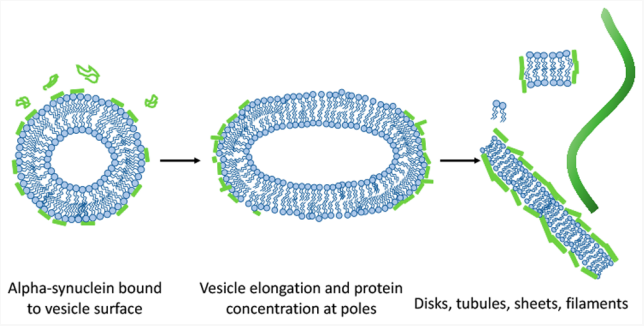

INTRODUCTION

Parkinson's disease is the second most common neurodegenerative disorder in the world, with an estimated 1 million patients in the United States and 10 million worldwide.[1,2] One defining characteristic of Parkinson's is the appearance of Lewy bodies, abnormal intraneuronal deposits comprised primarily of a 14 kDa protein, α-synuclein (aSyn), and lipid.[3−6] In Lewy bodies, aSyn is found as insoluble aggregates with a fibrillar morphology and cross-β-sheet structure typical of amyloid.[6] In vitro, the protein spontaneously aggregates into amyloid fibrils under certain conditions, such as with agitation or at acidic pH,[7,8] by a nucleation−elongation mechanism.[9]

In solution, aSyn is intrinsically disordered but adopts an elongated or broken α-helical secondary structure upon adsorption to lipid bilayers.[10−12] Generally, the amphipathic helix preferentially binds to lipid surfaces containing acidic headgroups,[10,11] to unsaturated lipids,[13] to membranes in the liquid disordered phase,[14,15] and to vesicles with high curvature.[11,14] Packing defects in the lipid bilayer, such as those introduced by high-curvature or conical lipid components, facilitate strong aSyn binding.[16,17] More broadly, the conserved amphipathic helix motif among the synuclein family of proteins has been identified as a region capable of both curvature sensing and curvature generation.[17−20] The latter action is believed to occur by lateral expansion of lipid headgroups via a wedging mechanism.[17−20]

While it is generally accepted that aSyn binding to biological membranes is essential for the protein to carry out its physiological function, interaction of the protein with lipid interfaces has also been found to promote its pathological aggregation under some circumstances.[15,21−25] For example, it has been demonstrated that lipid membranes composed of DMPS (1,2-dimyristoyl-*sn*-glycero-3-phospho-L-serine) stimulated the aggregation of aSyn.[15,24] A decrease in the acyl chain

Received: October 9, 2020
Revised: January 12, 2021
Published: February 4, 2021

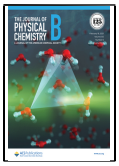

https://dx.doi.org/10.1021/acs.jpcb.0c09192
J. Phys. Chem. B 2021, 125, 1582−1594

length from DMPS (14:0) to DLPS (12:0) was found to further increase the rate of aSyn aggregation. By contrast, DOPS (18:1) vesicles did not stimulate protein aggregation, a finding attributed to its lower solubility.[15] The lipid surface can support a high local concentration of aSyn molecules, suggesting that protein crowding due to adsorption to the membrane may trigger aggregation. However, the stoichiometry and affinity of aSyn-vesicle binding were comparable for DOPS, DMPS, and DLPS vesicles,[15] suggesting that mechanisms beyond protein enrichment at the membrane surface must affect whether a specific lipid chemistry will stimulate aSyn aggregation.

The ability of aSyn to disrupt and promote changes in membrane shape and curvature has been well established for membranes composed of lipids with acidic phosphatidylglycerol (PG) head groups. Co-incubation of aSyn with model membranes consisting of POPG (1-palmitoyl-2-oleoyl-*sn*-glycero-3-phospho-1′-*rac*-glycerol), DMPG, and DLPG has been reported to disrupt vesicle integrity, resulting in conversion of spherical liposomes into a rich diversity of morphologies including tubules, cylindrical micelles, and thick bilayer tubes,[18,20,26,27] a process known as membrane remodeling. Membrane remodeling by aSyn has also been demonstrated with POPS and the zwitterionic POPC;[27,28] the latter case is somewhat surprising because the affinity of aSyn for POPC is low and aSyn remained in a disordered (non-α-helical) conformation. It has been previously suggested that aSyn-mediated membrane remodeling might influence aggregation under some circumstances.[27,28] For example, POPG tubules stimulated aSyn aggregation at a high protein:lipid ratio,[27] whereas POPC inhibited amyloid formation.[28] These studies were conducted by using mechanical agitation,[27,28] a treatment that accelerates aSyn aggregation in the absence of lipids.

In this investigation, we explored the role of aSyn-mediated membrane remodeling under quiescent conditions and at neutral pH. At these conditions, aSyn alone is not prone to aggregate; thus, the choice of these conditions allows any membrane remodeling to be isolated from confounding effects of aSyn aggregation or mechanical agitation. We chose PS because it is the predominant acidic headgroup in mammalian membranes and for direct comparison to a previous study in which PS lipid-mediated acceleration of aSyn aggregation was shown to be strongly and inversely dependent on acyl chain length, with greater stimulation of aggregation as chain length decreased.[15,24] In that work, aSyn aggregation was posited to occur on the membrane surface, without disruption of the lipid vesicles, and neither vesicle stability nor membrane remodeling was specifically interrogated.[15] Acyl chain length is physiologically relevant because peroxidation of polyunsaturated lipids shortens hydrocarbon chains, causing changes in membrane fluidity, increases in transport to other organelles, and cell damage.[24]

We used nanoparticle tracking analysis (NTA) to monitor changes in the properties of large unilamellar vesicles (LUVs) of DOPS (18:1) or DLPS (12:0) in the presence of aSyn. NTA is particularly useful for these studies as the technique allows simultaneous detection of particle size and particle number concentration over minutes to hours, in aqueous buffers, without the need for labels or dyes. With these data, along with images obtained by transmission electron microscopy (TEM), we demonstrate that the interaction of aSyn with DOPS LUVs induced a morphological change from spherical to ellipsoidal, but without significant vesicle lysis, fusion, or tubulation. In sharp contrast, interaction of aSyn with DLPS resulted in membrane remodeling into a polydisperse mixture of discoids, tubules, and helical ribbons, a process that continued for hours. Coarse-grained molecular dynamics simulations revealed that adsorption of aSyn to DLPS, but not DOPS, induced vesicle elongation that generated regions of high membrane curvature, leading to a preferential redistribution of aSyn molecules to the vesicle poles. These simulations provide insight into the mechanism by which aSyn induces major membrane remodeling in DLPS and may also explain how membrane remodeling could cause a high local protein concentration that may stimulate aggregation. Consistent with this hypothesis as well as previously published work, aSyn aggregation was much faster in the presence of DLPS compared to DOPS. Thus, the active response of lipid bilayers to aSyn adsorption depends on bilayer stability, and in turn membrane remodeling stimulates aSyn aggregation. Taken together, our results provide insight into α-synuclein's roles in membrane remodeling and membrane-mediated aggregation, thus connecting the protein's normal physiological function with its pathological one.

EXPERIMENTAL AND THEORETICAL METHODS

Purification of aSyn and Lipid Preparation. Wild-type aSyn was purified as described.[29] Lipids purchased from Avanti Polar Lipids Inc. (Alabaster, AL) were prepared in glass tubes under a gentle stream of nitrogen and evaporated overnight. Multilamellar vesicles (MLVs) were prepared by rehydration into phosphate-buffered saline (PBS: 10 mM NaH_2PO_4/Na_2HPO_4, 100 mM NaCl, pH 7.4). Large unilamellar vesicles (LUVs) were prepared by extrusion through a 100 or 50 nm polycarbonate membrane on a hot plate set above the phase transition temperature of the lipids. All experiments were conducted in PBS unless otherwise stated.

Vesicle Clearance Assay. Vesicle clearance of MLVs at protein:lipid (P:L) molar ratios of 1:40, 1:20, and 1:10 was monitored by using a spectrophotometer (Eppendorf) at a wavelength of 500 nm at room temperature. The total lipid concentration was 600 μM. Experimental details are provided in the Supporting Information.

Carboxyfluorescein Dye Leakage Assay. 5(6)-Carboxyfluorescein was encapsulated in 100 nm diameter LUVs, and dye leakage from vesicles (100 μM lipid) due to addition of aSyn (protein:lipid ratios of 1:1, 1:10, and 1:100) was monitored by excitation at 470 nm and emission at 525 nm with a QuantaMaster spectrofluorometer (PTI, Birmingham, NJ). Dye leakage was calculated as described in the Supporting Information.

Dynamic Light Scattering. aSyn (150 μM) and 100 nm DLPS vesicles (150 μM) in PBS were separately filtered through a 0.22 μm syringe filter (Millipore) before mixing into a precleaned quartz cuvette. The cuvette was placed into a bath containing refractive index matching decahydronaphthalene (Sigma) and equilibrated to 23 °C. Measurements were taken at a 90° scattering angle by using a Brookhaven BI-200SM and Innova 90C (Coherent, Inc.) 488 nm, 150 mW argon laser. Autocorrelation data were collected for 5 min following 24 h of co-incubation. A CONTIN fit to the autocorrelation function was used to determine a scattered intensity size distribution.

Nanoparticle Tracking Analysis. The kinetics of the interaction of aSyn with LUVs and the measurement of the hydrodynamic size and particle number concentration of DOPS or DLPS LUVs alone or with aSyn were monitored by

https://dx.doi.org/10.1021/acs.jpcb.0c09192
J. Phys. Chem. B 2021, 125, 1582−1594

NTA. All measurements were collected with a Nanosight LM10 (Nanosight) equipped with a 405 nm laser at room temperature for P:L molar ratios of 1:100, 1:10, and 1:1 for 5 h. Liposome samples were diluted to 6×10^9 liposomes/mL in 0.02 μm filtered PBS and mixed at P:L molar ratios of 1:1, 1:10, and 1:100 to obtain a concentration of $\sim 3 \times 10^9$ liposomes/mL at the start of data collection. Samples were injected directly into the sample chamber by using LuerLok syringes (BD). The camera level was maintained at a setting of 14. Video tracking was acquired for 30 s time intervals with five measurements for each sample. Measurements were repeated once per hour for 5 h. Analysis of the particle concentration, mean size, and standard deviation of particle tracks was conducted by using NTA 3.0 software using a detection threshold of 5. Additional information and calculations are provided in the Supporting Information.

Transmission EM. Samples were stained with a 2% solution of uranyl acetate on a 400 mesh copper grid. The grid was air-dried and imaged with a Techni T12 TEM at 120 V accelerating voltage at 1 s exposure time on a Gatan 4k Ultrascan CCD camera.

Coarse-Grained Molecular Dynamics Simulations. Simulations were performed by using the BMW MARTINI force field, which combines approximately four non-hydrogen atoms into single beads to model the interactions of protein, water, and lipids.[30,31] Simulations were performed at constant number of particles, pressure, and temperature by using GROMACS 2016. All simulations were performed at 87 °C to increase sampling without significantly influencing aSyn−bilayer interactions[32−34] and to decrease the bending rigidities of both membranes because BMW MARTINI overestimates lipid mechanical properties.[31,35,36] Similar elevated temperature simulations have been previously employed to model bilayer phenomena, including peptide partitioning into bilayers.[32,34] aSyn−vesicle systems were equilibrated for 120 ns followed by a production run of 300 ns. aSyn−bilayer systems were equilibrated for 200 ns followed by a production run of 700 ns. Both simulation workflows were repeated twice for each bilayer composition by using different initial velocities aSyn configurations. Detailed simulation methods are given in the Supporting Information.

Thioflavin-T (ThT) Assay. Kinetics of aggregation were monitored under two solution conditions: PBS and PB (20 mM NaH_2PO_4/Na_2HPO_4, pH 6.5). aSyn and lipid were mixed at a 1:10 P:L molar ratio and incubated at 37 °C in PBS for 8 days or at 30 °C in PB for 48 h. Aliquots containing 2 μM of protein were mixed with 10 μM of ThT and measured once per day. The aSyn concentration was 100 μM in PBS and 80 μM in PB. Fluorescence emission was monitored at an excitation of 440 nm and emission from 485 nm by using a QuantaMaster spectrofluorometer (PTI, Birmingham, NJ). An average of three independently prepared replicates and their standard error were determined by subtraction of the background fluorescence for a sample containing buffer only. The low background fluorescence at 0 h was subtracted from each later time point for each sample. For pelleted samples, 5 μL of resuspended pellet was mixed with 10 μM ThT, and the background with buffer alone was subtracted from the raw intensity.

Circular Dichroism (CD) Spectroscopy. aSyn and lipid were mixed at a 1:10 P:L molar ratio, 80 μM protein, in PB and incubated for 48 h at 30 °C. Samples were ultracentrifuged at 90K rpm for 30 min at 4 °C. The pellet was resuspended in PB. CD spectra of the supernatant, pellet, and background buffer were recorded between 185 and 340 nm by using an Aviv model 420 CD spectrometer. Data were acquired at room temperature with an averaging time of 5 s per wavelength. The molar protein concentration of the supernatant was determined by absorbance and that of the pellet by mass balance. The background buffer baseline was subtracted from the raw data and normalized by molar ellipticity.

RESULTS

Results are presented in the following order. We first present experimental data demonstrating that addition of monomeric aSyn induces much greater membrane disruption and remodeling of DLPS compared to DOPS vesicles. Next, coarse-grained molecular dynamic simulations are used to help elucidate the mechanisms underlying the experimentally observed differences in vesicle response to aSyn. Finally, we provide experimental data that correlates greater membrane remodeling of DLPS by aSyn to a greater potential of DLPS versus DOPS vesicles to induce aggregation of aSyn, an outcome that can be explained by protein-crowding phenomena identified by simulation.

Acyl Chain Length of PS Lipids Strongly Affects Vesicle Clearance in the Presence of aSyn. aSyn is well-known to bind strongly to phospholipids with acidic head groups, and under certain conditions, the binding leads to a loss of membrane integrity. Specifically, aSyn disrupts POPG multilamellar vesicles (MLVs), as detected by a decrease in turbidity over time by using a vesicle clearance assay.[18,37,38] The most prevalent acidic phospholipid in mammalian cell membranes is PS.[39] To determine whether aSyn disrupts PS membranes, we prepared MLVs of DOPS or DLPS (600 μM) with varying concentrations of aSyn and compared their vesicle clearance rates. Both lipids are in the fluid phase because the transition temperatures T_m are below the experimental temperature (T_m = 16 °C for DLPS versus −11 °C for DOPS). As shown in Figure 1, DOPS MLVs remained stable, while the turbidity of DLPS MLVs decreased rapidly with increasing aSyn concentration. This effect is not due to differences in the affinity of aSyn binding to DLPS versus DOPS, as the K_D's are similar.[15]

aSyn Induces Modest Changes in DOPS Liposome Shape and Permeability without Affecting Liposome Stability. Carboxyfluorescein (CF) was encapsulated in 100 nm DOPS large unilamellar vesicles (LUVs), and dye leakage was monitored by fluorescence following aSyn addition. The integrity of DOPS membranes was largely retained in the absence of protein (Figure S1). Addition of aSyn increased the rate of dye leakage in a concentration-dependent manner; dye leakage was gradual and incomplete, indicating the formation of transient and/or small pores or a subtle rearrangement of the protein−lipid interface upon protein adsorption.[40,41] TEM images were obtained of 100 nm DOPS LUVs alone or incubated for 5 h with aSyn at a protein:lipid (P:L) ratio of 1:10. DOPS LUVs alone were spherical, with a collapsed appearance typical of TEM images of unilamellar vesicles (Figure 2A). Binding of aSyn to DOPS induced changes in vesicle shape from spherical to prolate ellipsoidal (Figure 2B−D, white arrows).

To quantify changes in vesicle properties following the addition of aSyn, we used nanoparticle tracking analysis (NTA). In NTA, the Brownian motion of individual particles in solution is tracked to obtain the hydrodynamic diameter of

https://dx.doi.org/10.1021/acs.jpcb.0c09192
J. Phys. Chem. B 2021, 125, 1582−1594

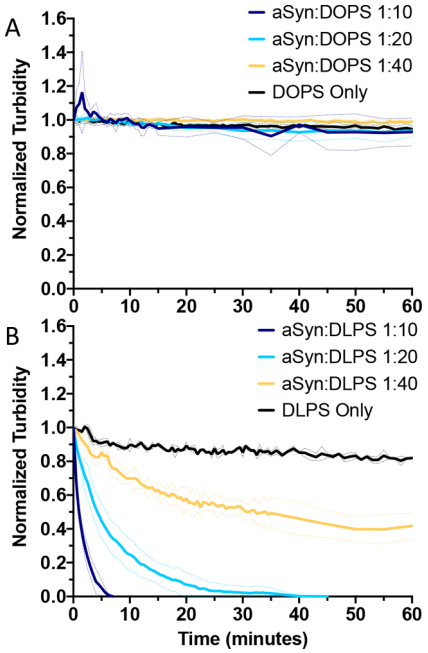

Figure 1. Propensity of aSyn to clear turbidity of solutions containing MLVs of model membranes. (A) Co-incubation of aSyn with DOPS MLVs. (B) Co-incubation of aSyn with DLPS MLVs. Experiments were conducted in PBS (10 mM phosphate buffer, 100 mM NaCl, pH 7.4) at 600 μM lipids with aSyn added at 1:40 to 1:10 P:L molar ratio at room temperature, above the phase transition temperature of both lipids. Data points indicate the average of three independent replicates, and shading indicates the standard deviation.

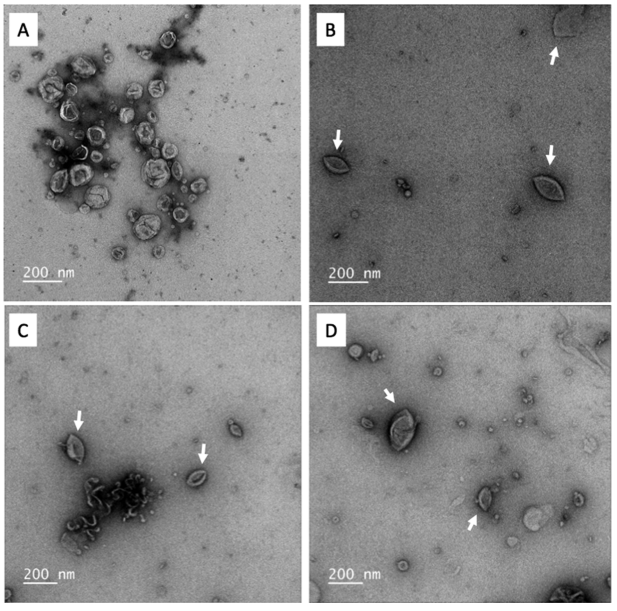

Figure 2. Effect of co-incubation of aSyn with DOPS membranes. Samples were prepared in PBS (pH 7.4). (A) TEM of DOPS LUVs alone or (B–D) with added aSyn at a 1:10 P:L molar ratio following 5 h of co-incubation at room temperature. Arrows indicate prolate ellipsoidal "football" vesicles. Images were taken from two independent replicates.

an equivalent sphere, D_{sphere}. The technique allows simultaneous measurement of the particle-by-particle size distribution as well as total particle number concentration. The minimum detection threshold for biological material is ~30 nm,[42,43] so monomeric aSyn (D_{sphere} ~ 5–6 nm)[44] is undetectable, and only the liposome or liposome–protein complex is sampled. A stock solution of DOPS LUVs of nominal 100 nm diameter was diluted to a particle number concentration optimal for analysis (3×10^9 liposomes/mL, ~500 nM lipid).[29] The number-weighted mean value of D_{sphere} of liposomes in the absence of protein was 103 ± 17 nm, averaged over three independently prepared replicates. Because the vesicle diameter and particle concentration varied somewhat for each independently prepared liposome solution, we normalized each subsequent measurement to the liposome-only value for that preparation. Samples of DOPS LUVs with aSyn at P:L molar ratios of 1:100, 1:10, and 1:1 were prepared and analyzed, with data collection continuing for 5 h. The mean normalized D_{sphere} increased immediately upon addition of aSyn, with little to no additional change thereafter (Figure 3A).

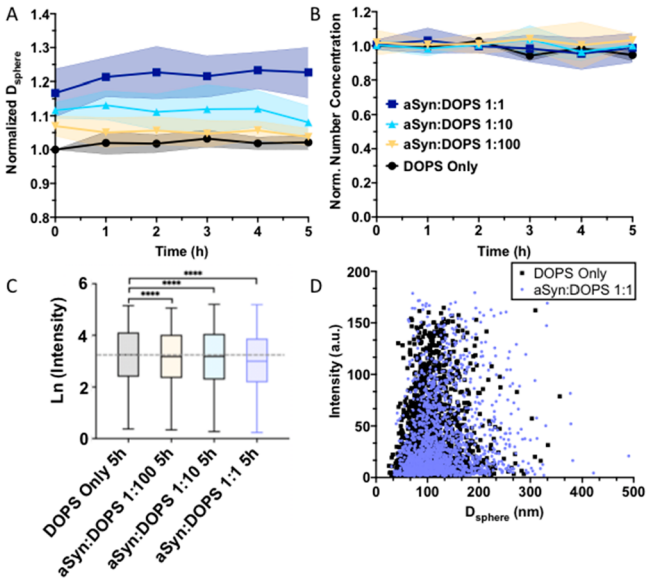

Figure 3. NTA analysis of DOPS LUVS (100 nm nominal size) alone or incubated with aSyn at 1:100, 1:10, or 1:1 P:L molar ratios. Samples were prepared in PBS and measurements taken at room temperature. (A) Number-averaged mean hydrodynamic diameter, normalized to LUVs alone at t = 0. Data points are the average of three replicates, and shading indicates the standard deviation. (B) Normalized particle number concentration. (C) Representative box-and-whiskers plot of the scattered intensity distribution for size range between 75 and 125 nm following 5 h of co-incubation. ****p < 0.0001 (unpaired two-tailed t test). Approximately 8000 particles per condition were tracked. (D) Representative comparison of particle size and scattered intensity distribution for DOPS alone (black) and with aSyn at 1:1 molar ratio (purple) after 5 h.

As the P:L ratio increased from 1:100, 1:10, and 1:1, D_{sphere} increased by approximately 7, 12, and 16 nm, respectively. The size of the increase is calculated for a single liposome preparation, with the increase similar across independently prepared liposome solutions despite some variability in absolute liposome size between different preparations. A representative particle-by-particle size distribution is shown in Figure S2, exhibiting a unimodal distribution with a shift toward larger diameter upon aSyn addition. There was no change in liposome number concentration upon addition of aSyn (Figure 3B), indicating that the liposomes remained stable, with no indication of vesicle fusion or breakup.

https://dx.doi.org/10.1021/acs.jpcb.0c09192
J. Phys. Chem. B 2021, 125, 1582–1594

We evaluated whether the increase in D_{sphere} was fully accounted for by adsorption of aSyn to the interface. It is generally accepted that aSyn adopts an α-helical conformation upon binding to lipid bilayers and that the bulk of the protein rests on the surface of the membrane,[45,46] sampling between an extended single helix or a broken helix conformation.[47] We estimated the thickness of a monolayer of aSyn bound to liposomes to be that of an α-helix (~1.2 nm),[48] with a small unknown additional contribution from the disordered C-terminal tail.[49] Thus, aSyn adsorption as a monolayer to the surface should increase D_{sphere} of liposomes by only ~3 nm, insufficient to explain the entire observed 7−16 nm increase. We wondered whether the "excess" increase in D_{sphere} (beyond that expected by adsorption) could be explained by the aSyn-mediated induction of a shape change from spherical to ellipsoidal that was observed in TEM images. To test this, we measured the dimensions of 45 liposomes in the absence of aSyn (Figure 2A) and obtained a diameter of 94 ± 27 nm. Next, the major and minor axial dimensions of 20 prolate ellipsoids formed in the presence of aSyn, similar to those observed in Figure 2B−D, were measured to be 130−175 nm and 75−100 nm, respectively. Using a model for the hydrodynamic diameter of prolate ellipsoids (Supporting Information), we calculated D_{sphere} = 110 ± 40 nm, or an increase of 16 nm in the mean hydrodynamic diameter. This result is in good agreement with the increase in diameter measured by NTA following the addition of protein. We repeated the NTA experiment with DOPS liposomes extruded through a 50 nm membrane and observed a comparable trend, but with a smaller increase in size (Figure S3). If adsorption alone without a shape change could account for the increase in D_{sphere}, then the size of the increase should be independent of the LUV diameter. This result is consistent with our interpretation of NTA and TEM data—that adsorption of aSyn to DOPS liposomes induces a change in shape from spherical to slightly ellipsoidal.

NTA provides not only size and number information but also intensity of scattered light on a particle-by-particle basis. The intensity distribution of the incident light is broad because the beam is Gaussian. The scattered intensity per particle I_p varies with the intensity of the incident beam I_0 and is a function of particle molecular weight M, refractive index increment dn/dc, and particle scattering factor $P(q)$, which depends on particle shape and dimensions[50,51]

$$I_p \propto I_0 M^2 \left(\frac{dn}{dc}\right)^2 P(q) \quad (1)$$

Upon aSyn binding to liposomes, I_p should increase because M of the protein−liposome complex is greater than that of liposome alone and because dn/dc for protein (0.19 mL/g)[52] is larger than for lipid (0.16 mL/g).[53] Countering this effect, a change in shape from spherical to ellipsoid reduces $P(q)$ and therefore decreases I_p; we calculated an ~10% reduction in $P(q)$ based on the dimensions from TEM (Supporting Information). We analyzed scattering from ~8000 particles with D_{sphere} between 75 and 125 nm. We observed a small but statistically significant decrease in the mean intensity of the population for DOPS + aSyn relative to DOPS only (Figure 3C,D, Figures S4 and S5), consistent with the change in vesicle shape from spherical to ellipsoidal.

Taken together, dye leakage, NTA, and TEM results show that aSyn modestly increases membrane permeability of DOPS LUVs and changes the shape from spherical to ellipsoidal but does not cause vesicle breakup or major vesicle disruption.

aSyn Substantially Disrupts and Remodels DLPS Liposomes. We verified by NTA that DLPS LUVs were formed during extrusion of lipids with a measured diameter of ~100 nm (not shown). However, we were unable to encapsulate CF inside DLPS vesicles, indicating that DLPS vesicles are inherently less cohesive than DOPS vesicles. Lack of dye retention has also been reported for DLPC membranes[54] and is attributable to the lipid's finite solubility (100 nM).[15]

We diluted DLPS LUVs to ~3×10^9 liposomes/mL (~500 nM lipid) and investigated their properties by NTA. Whereas DOPS vesicles were stable upon dilution, the size and number concentration of DLPS vesicles slowly decreased over several hours (Figure 4A,B, black). This outcome is consistent with

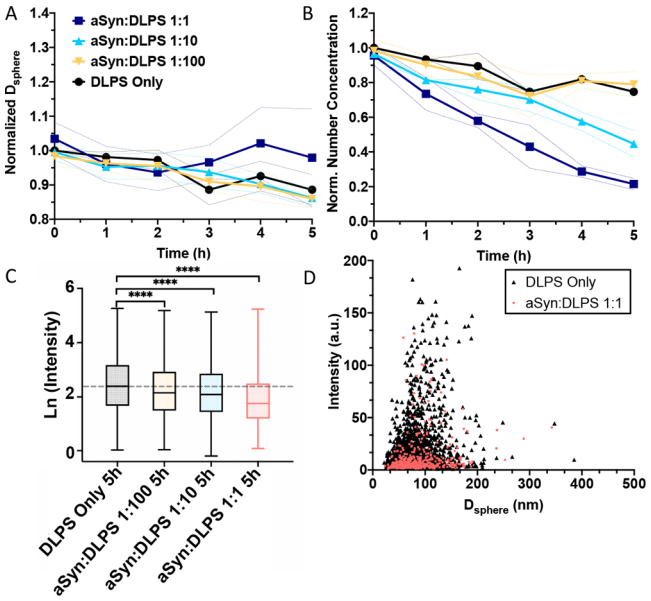

Figure 4. NTA analysis of DLPS LUVS (100 nm nominal size) alone or incubated with aSyn at 1:100, 1:10, or 1:1 P:L molar ratios. Samples were prepared in PBS, and measurements were taken at room temperature. (A) Number-averaged mean hydrodynamic diameter, normalized to LUVs alone at t = 0. Data points are average of three replicates, and shading indicates standard deviation. (B) Normalized particle number concentration. (C) Representative box-and-whiskers plot of the scattered intensity distribution following 5 h of co-incubation. Approximately 15000 DLPS vesicles in the absence of lipid were tracked and compared with ~14500 (P:L 1:100), ~9700 (P:L 1:10), and ~4400 (P:L 1:1) particles. ****$p < 0.0001$ (unpaired two-tailed t test). (D) Representative comparison of particle size and scattered intensity distribution for DLPS alone and with aSyn at 1:1 molar ratio after 5 h.

partial dissociation of liposomes upon dilution due to the finite DLPS solubility. We then measured the effect of aSyn addition on DLPS LUVs for P:L molar ratios of 1:100, 1:10, and 1:1. Whereas vesicle size increased with aSyn addition for DOPS, the normalized D_{sphere} decreased slightly over time for both DLPS alone and at 1:100 and 1:10 P:L (Figure 4A). At 1:1 P:L, D_{sphere} was nearly constant with time, but there was high variability in the data. Also, in sharp contrast to the unchanging particle number concentration upon addition of aSyn to DOPS, the particle number concentration decreased significantly with time, with the rate of change increasing with

https://dx.doi.org/10.1021/acs.jpcb.0c09192
J. Phys. Chem. B 2021, 125, 1582−1594

protein concentration and the decrease continuing over the entire 5 h measurement period (Figure 4B). Particle size distributions of DLPS with and without aSyn revealed overall similar size distributions but with the addition of a few very large particles at 1:1 P:L following 5 h (Figure S6). Mean I_p decreased significantly as P:L molar ratio increased (Figure 4C, Figures S7 and S8); the change was much greater for DLPS than for DOPS. The decrease in I_p is also apparent in the intensity distribution plot (Figure 4D) and was time-dependent at all P:L molar ratios (Figure S8).

TEM images of mixtures of aSyn with DLPS were obtained to assist with further interpretation of NTA results. These images revealed a striking morphological diversity, including twisted and helical ribbons (Figure 5A–C), tubules (Figure 5D), and discoids (Figure 5E–G), all of which were absent in control vesicles (Figure 5H). The most numerous objects were flattened discoids ~30 nm in diameter and 5 nm in thickness (Figure 5E–G). Tubules (Figure 5D) were typically 10–20 nm in diameter with contour lengths ranging between 300 and 700 nm. Larger structures (~1.5 μm in length) were rare but consistently observed in multiple preparations.

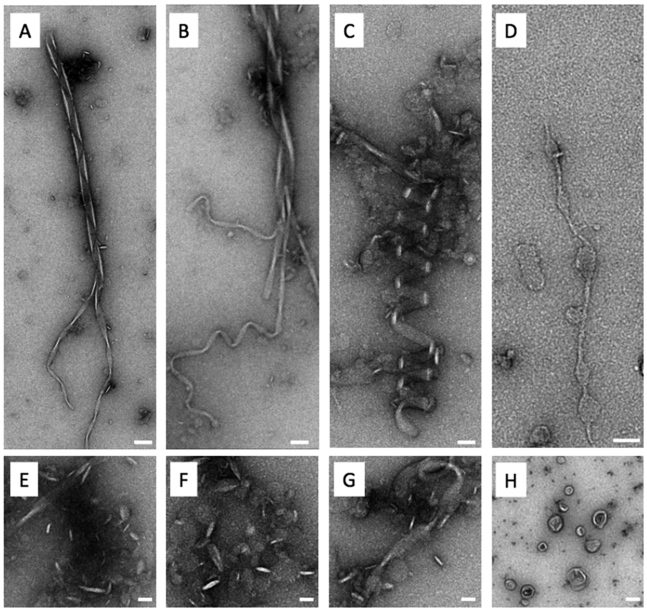

Figure 5. Effect of co-incubation of aSyn with DLPS membranes. (A, B) TEM images exhibiting large twisted and helical ribbons. Scale bar is 100 nm. (C) Helical ribbon. Scale bar is 50 nm. (D) Thin tubules. Scale bar is 100 nm. (E–G) Discoid shapes. Scale bar is 50 nm. (H) DLPS vesicles in the absence of aSyn. Scale bar is 100 nm. Samples were prepared in PBS and incubated for 5 h at room temperature. Images were taken from two independent replicates.

As a negative control, addition of bovine serum albumin did not cause any vesicle remodeling or shape change in DLPS or DOPS, as assessed by both TEM and NTA (Figure S9). This result indicates that vesicle remodeling is specific to aSyn and not a general property of protein interaction with these vesicles.

We tested whether the decrease in particle number concentration as measured by NTA could be attributed to vesicle breakup into small discoids. We obtained dimensions of 47 discoids from TEM images and calculated D_{sphere} for these particles to be 27 ± 7 nm (Supporting Information), a size slightly below the minimum size detection threshold of the instrument of about 30 nm. We confirmed this detection threshold by using IgM, an oblate ellipsoid with hydrodynamic diameter of ~28 nm.[29] To find additional evidence for the existence of these smaller particles, we measured the size distribution of aSyn–DLPS mixtures using dynamic light scattering (DLS), a technique that provides average rather than particle-by-particle size measurements but is sensitive to much smaller particles compared to NTA. An analysis of the autocorrelation function indeed revealed a bimodal size distribution with peaks centered near 25 and 100 nm (Figure S10). Taken together, this analysis supports our interpretation that the NTA-measured decrease in particle number concentration can be attributed, at least in part, to break up into small discoids.

We next considered the tubules. To estimate their hydrodynamic properties from dimensions derived from TEM images, we used a semiflexible (wormlike) chain model. We measured contour lengths of 300–700 nm and diameters of 10–20 nm (Supporting Information), yielding an estimate of D_{sphere} of 60–100 nm, in reasonably good agreement with the particle sizes detected by NTA as well as the second peak in the particle size distribution obtained by DLS. From tubule dimensions, we calculated the number of lipids per tubule, as well as the number of lipids in a 100 nm diameter sphere, and concluded that a tubule could form by remodeling of a single vesicle (Supporting Information). To interpret the decrease in I_p upon addition of aSyn (Figure 4C), we calculated $P(q)$ of 0.36–0.64 for tubules of 300–700 nm length compared to 0.98 for LUVs (Supporting Information). The slow continuing decrease in I_p with time (Figure S8) suggests that aSyn remodeling of LUVs to tubules occurs slowly and continues for hours.

The hydrodynamic properties of the rare helices and ribbons are difficult to calculate; as a rough estimate we calculated D_{sphere} ~ 375 nm using a hollow cylinder model for the morphology shown in Figure 5A, which has a length of ~1500 nm and diameter of ~70 nm. There are indeed a few particles detected by NTA that are in this size range. Given the large dimensions of these particles, they must arise from fusion of many vesicles, which would also lead to a decrease in number concentration. As a final note, we have previously observed that thin, highly elongated particles are undercounted by NTA, a phenomenon that can be explained by interference effects,[50,51] which would also lead to a decrease in number concentration over time.

Taken together, our combined data are consistent with a remarkable degree of aSyn-induced remodeling of DLPS vesicles into a diversity of morphologies ranging from discoids (a product of vesicle breakup) to tubules (vesicle rearrangement) to large ribbons and coils (vesicle fusion and restructuring). Moreover, membrane remodeling is a slow process that continues over hours.

Coarse-Grained Simulations Identify Differences in aSyn Interactions with DOPS versus DLPS. We performed coarse-grained molecular dynamics (MD) simulations using the BMW MARTINI force field to gain molecular insight into the interactions of aSyn monomers with DOPS and DLPS vesicles. This force field permitted simulations of sufficiently large system sizes to observe membrane remodeling while reproducing electrostatics effects that could influence aSyn binding.[30,31,55] BMW MARTINI has also been shown to reproduce membrane adsorption behavior observed in more detailed all-atom simulations and experiments.[31,56,57] We first

https://dx.doi.org/10.1021/acs.jpcb.0c09192
J. Phys. Chem. B 2021, 125, 1582–1594

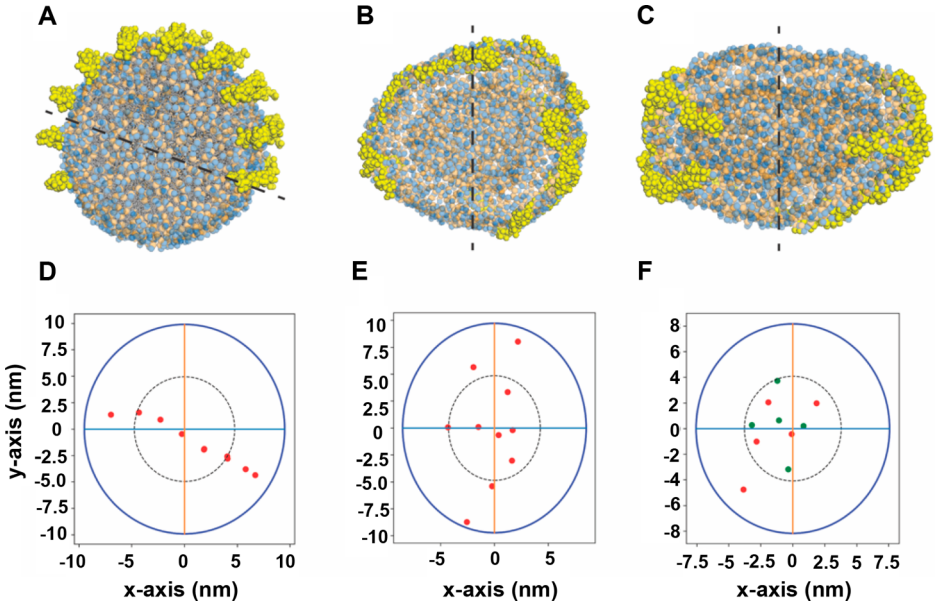

Figure 6. MD simulations of aSyn interaction with DOPS or DLPS vesicles. (A) Initial configuration of 10 aSyn monomers placed near a vesicle surface. (B) DOPS vesicle after equilibration. (C) DLPS vesicle after equilibration. The dashed lines in (B) and (C) indicate the equatorial plane of each vesicle. (D–F) Stereographic projections of the location of the 10 aSyn monomers with respect to the equatorial plane for the simulation snapshots in (A–C). In (F), aSyn monomers above and below the equatorial plane are labeled with green and red points, respectively.

modeled aSyn binding to small vesicles to determine whether the simulations predict morphology changes that were consistent with our experiments. We self-assembled single-component DOPS and DLPS vesicles (diameters of 9.6 and 9.8 nm, respectively) in the absence of aSyn and then placed 10 evenly spaced aSyn monomers in solution 2 nm from the outer leaflet of each vesicle (Figure 6A,D and Figure S11) and allowed the monomers to adsorb to the vesicles in unbiased MD simulations. Simulation of the larger vesicles used in experiments (~100 nm) while maintaining a chemically specific force field such as MARTINI is not computationally tractable. As controls, we also simulated DOPS and DLPS vesicles in the absence of aSyn with the same simulation parameters. All simulation systems (described in the Supporting Information and Table S1) were simulated twice with different initial configurations and velocities.

The simulations revealed that all 10 aSyn monomers rapidly bind to both vesicles. aSyn binding led to minimal change in the structure of a DOPS vesicle compared to the control (Figure 6B), and the aSyn monomers distributed in clusters with no apparent order on the vesicle surface. The monomer distribution for the final simulation configuration is illustrated by stereographic projections that plot the center-of-mass (COM) positions of the monomers relative to the equatorial plane of the vesicle (Figure 6E). In contrast, aSyn binding induced the elongation of a DLPS vesicle and the accumulation of monomers at the poles of the elongated structure (Figure 6C,F). To quantify the extent of deformation of each vesicle from a sphere, we compared the meridional and equatorial eccentricities (Figure S12 and Table S2), calculated as $e = \sqrt{1 - b^2/a^2}$, where a and b represent the semimajor and minor axes, respectively. The meridional eccentricity of the DLPS vesicle (0.78 ± 0.01) was much greater than that of the DLPS vesicle in the absence of aSyn (0.49 ± 0.06), while the equatorial eccentricity (0.34 ± 0.08) is similar to that in the absence of aSyn (0.32 ± 0.09). Both the meridional (0.59 ± 0.03) and equatorial (0.36 ± 0.08) eccentricities of the DOPS vesicle increased compared to the DOPS vesicle control (0.38 ± 0.06 and 0.25 ± 0.07, respectively), but to a much lesser degree than the increase of meridional eccentricity of the DLPS vesicle. These results confirm that aSyn binding slightly perturbs the structure of DOPS while significantly elongating the DLPS vesicle. While the simulated vesicles are substantially smaller than those studied experimentally to be computationally tractable, these simulation findings are consistent with our experimental observations of a minor deformation of DOPS vesicles and the more pronounced remodeling of DLPS vesicles.

We hypothesized that the difference in the morphology in DOPS vesicles versus DLPS upon adsorption of aSyn arose because of differences in the curvature induced by aSyn binding. To interrogate this hypothesis, we modeled the interactions of a single aSyn monomer with a planar DOPS or DLPS bilayer. To quantify induced curvature, we calculated the change in the time-averaged height of the lipid surface near the bound aSyn monomer (Supporting Information). aSyn binding to a planar DOPS bilayer increased the height of the lipid interface around the bound protein parallel to its long axis (Figure S13, Figure S14, and Table S3). This result indicates that aSyn induces local positive curvature in flat DOPS bilayers, consistent with previous reports,[37] suggesting that aSyn preferentially binds to positively curved and not flat DOPS bilayers which would tend to stabilize the spherical vesicles. On the other hand, aSyn binding to a planar DLPS membrane led to a smaller increase in the height of the lipid interface relative to the DOPS results, indicating a preference for flatter bilayers with less positive curvature. The response of planar bilayers to aSyn adsorption explains the behavior observed in the vesicle simulations: aSyn binding to the DLPS bilayer flattens the local bilayer curvature, thus driving elongation, because elongation flattens the bilayer along one axis.

The simulations also suggest that aSyn monomers preferentially, although not exclusively, accumulate at the

https://dx.doi.org/10.1021/acs.jpcb.0c09192
J. Phys. Chem. B 2021, 125, 1582–1594

poles of elongated DLPS vesicles (Figure 6C). However, this accumulation was less apparent in a second simulation (Figure S15). We performed additional simulations in which a single monomer diffused on a DLPS vesicle that was restrained in an elongated conformation (Figure S16). In two independent simulations, the monomer aligned its long axis parallel to the long axis of the elongated vesicle and diffused toward the pole. These simulations confirm that the accumulation of aSyn monomers at the poles reflects curvature sensing rather than direct monomer−monomer interactions. Combined, these simulations suggest that there are two apparently contradictory outcomes of aSyn−DLPS interactions: aSyn adsorption tends to flatten and therefore elongate DLPS vesicles, but on the other hand, adsorbed aSyn tends to migrate toward the highly curved poles. In the simulation snapshots of Figure S14, migration of an aSyn monomer leads to the disordered tail region (green) binding to the highly curved pole, in agreement with recent simulations indicating that the disordered tail can contribute to curvature.[58] Together, these observations suggest that curvature generation versus curvature sensing could emerge from different conformations of bound aSyn monomers.

Aggregation of aSyn Is Stimulated by DLPS but Not DOPS. Simulation results suggest that aSyn binding can trigger vesicle shape change in DLPS and local accumulation of aSyn monomers at regions of high curvature, which might lead to aggregation. Several groups have shown that under certain conditions lipids can accelerate aSyn aggregation.[15,21,22,24,25] Of particular relevance, Galvagnion et al. reported that DLPS but not DOPS induced aggregation of aSyn at pH 6.5 in the absence of added salt, while DMPS was intermediate in its ability to cause aSyn aggregation.[15] We incubated aSyn with DOPS, DMPS, or DLPS LUVs and tested for the formation of amyloid fibrils using the thioflavin T (ThT) fluorescence assay. Samples were incubated in PBS (pH 7.4, 100 mM NaCl) at 30 and at 37 °C. At 30 °C we did not observe any aggregation during the course of the study. At 37 °C after 168 h, a significant increase in ThT fluorescence was observed in DLPS, a smaller increase in DMPS, and virtually no increase in DOPS, while the protein-only control remained ThT-negative (Figure 7A). We repeated the experiment in PB (pH 6.5, 0 mM NaCl) and 30 °C to mimic the conditions used in previously published work.[15] Lowering the salt concentration and pH increased the rate of aggregation significantly, as expected, but did not change the order of lipid dependence (Figure 7B). TEM images were taken of aSyn in the presence of DOPS, DMPS, and DLPS after 4, 24, or 48 h of incubation in PB (Figure 7C−E and Figure S17). With DOPS vesicles, the TEM images revealed some incipient tubulation at 5 h and disruption of intact vesicles at 48 h, but no large ribbons or helical coils were observed (Figure 7C). In contrast, with DLPS, significant membrane lysis was evident at 5 h alongside examples of twisted and helical ribbons, with a higher frequency at 24 h (Figure 7E). Similar morphologies, although less frequent, were observed with DMPS (Figure 7D). Comparable morphologies and positive ThT fluorescence were also observed in aSyn mixed with DLPG liposomes (Figure S18). Thus, there is a strong correlation between the appearance of twisted and helical ribbons and an increase in ThT fluorescence.

Identically prepared samples were incubated for 48 h. Samples were centrifuged, and then the resuspended pellet and supernatant were analyzed separately for protein and lipid

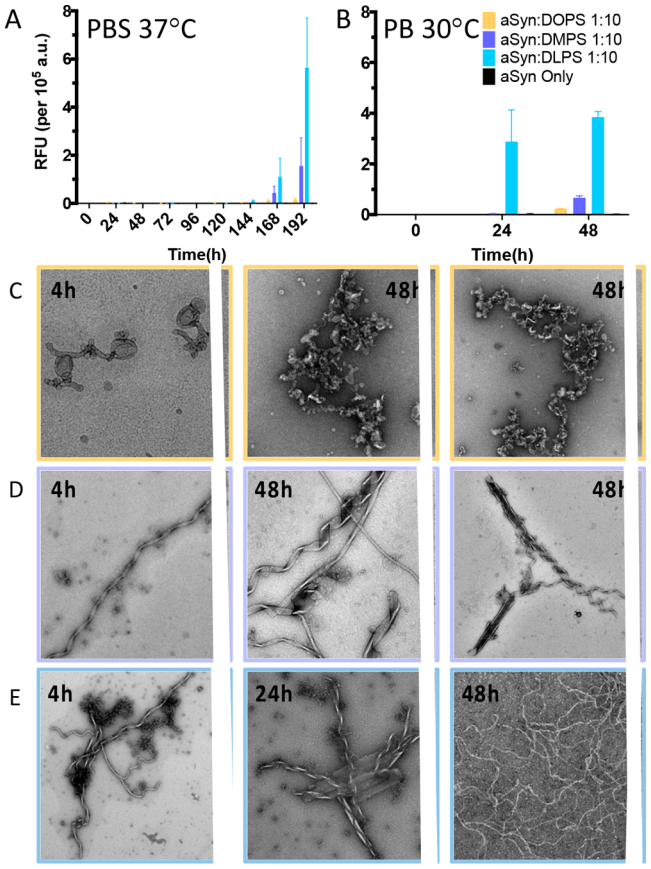

Figure 7. Aggregation propensity and morphology of aSyn incubated in the presence of model membranes. (A) ThT fluorescence of aSyn alone (black, 100 μM) or with DOPS (orange), DMPS (purple), and DLPS (blue) at a P:L molar ratio of 1:10 in PBS. (B) ThT fluorescence for the same P:L molar ratio (80 μM:800 μM) in PB (pH 6.5). Data represent the average of three independent replicates, and error bars indicate the standard error of the mean. (C−E) TEM images showing representative examples of morphologies observed in the presence of (C) DOPS, (D) DMPS, and (E) DLPS at the indicated time points in PB. Scale bars are 100 nm in all images.

content (Table S4 and Figure S19), imaged by TEM (Figure 8A−D), and analyzed for secondary structure by circular dichroism (CD, Figure 8E). The resuspended DOPS pellet contained primarily intact vesicles with some minor tubulation (Figure 8A). CD spectra were consistent with α-helical secondary structure (Figure 8E), typical of aSyn bound to lipid vesicles (59), and the ThT signal was weak, indicating that the vast majority of aSyn remains lipid-bound in a nonfibrillar form with DOPS. With DLPS, about 10% of protein and lipid were found in the pellet (Table S4). The resuspended pellet contained a polydisperse mixture of morphologies including tubules, ribbons, and tapes (Figure 8C,D); CD spectra exhibited a broad minimum at ∼215−218 nm (Figure 8E), characteristic of β-sheet secondary structure that is typical of amyloid aggregates,[59] and the pellet was strongly ThT-positive. In contrast, no coils, ribbons, or sheets were observed in the DLPS supernatant (Figure S19C), and CD spectra of the supernatant indicated an α-helical conformation (Figure S19D). This result indicates that a fraction of aSyn is responsible for fibril formation in the presence of DLPS vesicles, while most of the protein remains lipid-bound but not aggregated. Thus, the presence of tubules, ribbons, and tapes is associated with the formation of β-sheet

https://dx.doi.org/10.1021/acs.jpcb.0c09192
J. Phys. Chem. B 2021, 125, 1582−1594

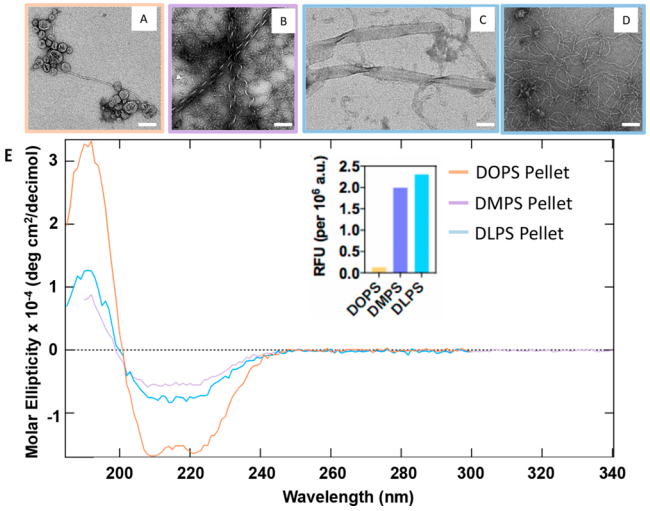

Figure 8. TEM images and CD spectra of resuspended pellets following co-incubation of aSyn and vesicles. (A–D) Samples (P:L 1:10) were incubated in PB for 48 h at 30 °C and pelleted by ultracentrifugation. The supernatant was removed, and the pellets were resuspended. TEM images of aSyn with DOPS (orange), DMPS (purple), and DLPS (blue). Scale bar is 100 nm for (A, B, and D) and 50 nm for (C). (E) Circular dichroism spectra. Inset shows ThT fluorescence of the pellet following CD.

and amyloid (ThT-positive) structures. Similarly, the resuspended DMPS pellet contained twisted and helical ribbons (Figure 8B) and CD spectra as well as ThT fluorescence indicated β-sheet secondary structure (Figure 8E), again demonstrating a strong correlation between aSyn-induced membrane remodeling and the conversion of aSyn to β-sheet amyloid aggregates.

DISCUSSION

Our investigation was motivated by reports that aSyn aggregation was strongly promoted by DLPS but not DOPS vesicles, despite similar adsorption properties.[15] Using both experiment and simulation, we studied the response of DLPS and DOPS vesicles to aSyn adsorption, prior to the onset of aSyn aggregation. Because of its shorter acyl chain and greater lipid solubility, DLPS vesicles are unstable compared to DOPS vesicles, as evidenced by their inability to encapsulate dye and the slow decrease in vesicle number upon dilution even in the absence of aSyn (Figure 4B). We hypothesized that the lower intrinsic stability of DLPS vesicles would lead to a much stronger remodeling response to aSyn. Indeed, as shown by a combination of NTA, TEM, and dye leakage assays, the interaction of aSyn with DOPS LUVs resulted in a modest change in vesicle shape from spherical to ellipsoidal, but without significant vesicle fusion, tubulation, or lysis. In sharp contrast, interaction of aSyn with DLPS LUVs led to the formation of a rich heterogeneity of morphologies, including discoids, tubules, and large twisted and helical ribbons.

A novel feature of our work is the combination of NTA and TEM to investigate the response of liposomes to aSyn. Advantageous features of NTA are that the kinetics of membrane remodeling can be followed over time, and information about vesicle size, number, and shape is obtained simultaneously, in real time, and without the use of labels, dyes, or other reagents. Through NTA, we observed that the increase in size of DOPS LUVs upon addition of aSyn was essentially instantaneous, and vesicle size did not change further over 5 h. The constant particle number concentration, as well as the immediate change to a lower scattering intensity, is consistent with a small shift in particle morphology from spherical to ellipsoidal upon aSyn adsorption to DOPS, as evidenced by TEM images. On the other hand, membrane remodeling of DLPS is an extensive and slow process that continues unabated over several hours, a conclusion consistent with the continued decrease over time in measured particle number concentration (Figure 4B) and scattered intensity (Figure S8). Discoids and tubules were the most numerous remodeled species in mixtures of aSyn with DLPS (Figure 5D–F and Figure S10). Discoids are likely the product of pinching off patches of membrane, while tubules likely arise from major restructuring of a single vesicle (Supporting Information).

Through coarse-grained MD simulations, we identified a mechanism by which aSyn induces greater remodeling in DLPS compared to DOPS vesicles, recognizing that simulations can capture only the earliest steps in the remodeling process. Specifically, aSyn binding generated greater positive curvature in planar DOPS bilayers compared to DLPS bilayers, which indicates that aSyn would tend to stabilize sphericity in DOPS to a greater extent than DLPS. Indeed, aSyn binding to spherical DLPS vesicles led to elongation of vesicles to create a long axis with a reduced radius of curvature. The more dramatic remodeling of DLPS compared to DOPS is facilitated by the lower bending rigidity of DLPS bilayers due to its shorter tail. These lipid-dependent curvature preferences are consistent with the dominant remodeled DLPS structures observed by TEM: tubules and discoids have reduced curvature along one (tubule) or two (discoid) axes compared to spheres. Interestingly, aSyn monomers were found to preferentially redistribute toward the higher curvature poles of the elongated DLPS vesicles, with migration to the pole associated with an oriented binding of the disordered tail region. Thus, our simulations indicate that aSyn monomers act as both curvature *modifiers* to drive lipid-dependent membrane remodeling processes[60] and as curvature *sensors* to facilitate protein-mediated crowding. These results are in broad agreement with MD simulations of other curvature-sensing and generating proteins; for example, one study showed that N-BAR domains exhibited a preference for curvature and, at ∼50% bound protein density, led to significant local protein crowding.[61] Although more detailed investigations are required to confirm the mechanism underlying these phenomena, these observations suggest that curvature generation versus curvature sensing could emerge from different conformations of bound aSyn monomers, which also may contribute to diverse remodeled structures observed experimentally.

In addition to numerous discoids and tubules in the DLPS samples, we observed larger structures such as sheets, twisted and helical ribbons, and nanotubes (Figure 5A–C, Figure 7E, and Figure S17). These morphologies occurred only in the presence of aSyn and resemble aggregates formed from self-assembling peptides[62] and selected peptide sequences from amyloidogenic proteins,[63,64] including an amphiphilic eight-residue peptide of aSyn.[65] Generally, the ribbons, tubes, and sheets appeared prior to the detection of amyloid by ThT. TEM, CD, and ThT results provide a strong linkage between the formation of these morphologies, adoption of β-sheet secondary structure, and amyloid formation (Figure 8). Although we did not directly test whether the aggregates we

https://dx.doi.org/10.1021/acs.jpcb.0c09192
J. Phys. Chem. B 2021, 125, 1582–1594

observed contained both lipid and protein, the similarity in the fraction of protein and lipid in pelletable fractions (Table S4) suggests that coassembly likely underlies their formation. These results are consistent with recent studies that have also demonstrated coassembly of protein and lipid after prolonged incubation.[27,66] Compositional and structural characterization of the discoids, tubules, and large ribbons and coils formed upon co-incubation of aSyn and DLPS is beyond the scope of the current investigation but would provide further insight into their nature and mechanism of formation.

Local enrichment of protein molecules by adsorption to surfaces is one mechanism by which aSyn aggregation might be accelerated. Experimental support for this hypothesis has been inferred from NMR data that showed molecular crowding of aSyn on the surface of flat nanodiscs, resulting in close spatial proximity of the NAC region that is necessary for aggregation.[67] Our simulations point to a story in which aggregation arises from active responses of aSyn and lipid vesicle to each other. Adsorption of aSyn to a lipid vesicle of low bending rigidity like DLPS drives vesicle elongation, producing regions of variable curvature. Then, the protein redistributes to and concentrates in the polar regions of the elongated vesicle. In other words, membrane remodeling induced by aSyn provides the conditions that lead to aSyn crowding and then, presumably, aSyn aggregation.

Whether membrane-remodeling stimulation of aSyn aggregation is a general phenomenon remains an open question. A strong correlation between reduced vesicle integrity (greater lipid solubility) and increased stimulation of aSyn aggregation was observed with PS lipids of variable chain length, but membrane remodeling was not interrogated and it was assumed that aggregation occurred on stable vesicle surfaces.[24] Vesicle clearance, tubulation, and vesicle leakage were reported upon addition of aSyn to POPG but not POPC,[18,19] but aSyn aggregation was not measured in that study. Similarly, micelles, tubules, and discoids were observed with PG vesicles, with morphological differences depending on the protein:lipid ratio and length of the acyl chain,[26] but again aggregation was not explored. In pioneering work, Lee and co-workers directly explored the relationship between membrane remodeling and aSyn aggregation.[27,28] Briefly, POPG and POPS were remodeled by aSyn into micellar tubules, and POPG tubules stimulated aSyn aggregation at high but not low protein:lipid ratios; POPS was not tested for its effect on aggregation.[27] In another study, these researchers reported an inverse relationship between membrane remodeling and aSyn aggregation: specifically, vesicles of POPC but not POPC/POPA were tubulated by aSyn, whereas aSyn aggregation was inhibited by POPC and stimulated by POPC/POPA.[28] Interestingly, the binding affinity of aSyn for POPC is much weaker than for lipids with acidic head groups, and aSyn remained disordered and not α-helical when mixed with POPC, so aSyn-induced tubulation of POPC was a somewhat surprising result. The underlying reason for the different relationship between membrane remodeling and aSyn aggregation stimulation in that work versus in our work is unknown. One possible difference is the difference in headgroup charge, since PA and PS are acidic but PC is zwitterionic. Another is that Lee and co-workers used mechanical agitation which promotes aSyn aggregation in the absence of lipids,[8,68,69] whereas our experiments were conducted quiescently, under conditions where aSyn alone did not aggregate. In preliminary studies, we observed disruption of DOPS LUVs increased strongly with an increase in shaking intensity, and this disruption correlated to an increase in ThT fluorescence when co-incubated with aSyn (Hoover and Murphy, unpublished observations).

Taken together, our results demonstrate aSyn-mediated membrane remodeling as a precursor to membrane-mediated aSyn aggregation. Phospholipid compositions that reduce bilayer rigidity and membrane stability could facilitate active aSyn-mediated membrane remodeling, likely a key feature of the protein's normal biological function, but may also conversely facilitate pathological aggregation. Thus, age-related changes in lipid composition, such as a greater abundance of shorter fatty acid tails, that lead to reduction in membrane integrity may be important contributors to aSyn aggregation and Parkinson's disease etiology. In agreement with this view, it has recently been identified that Lewy body pathology is characterized by a much larger lipid content than previously thought,[3,4] with an abundance of vesicular structures, dysmorphic organelles, membranous fragments, and crowding of aSyn and lipid in Lewy bodies and neurites.[5] Describing the process by which lipid and protein are reorganized into the morphologies identified in this study will be important in understanding the role of lipid in modulating aSyn aggregate structure and pathology *in vivo*.

CONCLUSIONS

Using nanoparticle tracking analysis along with electron microscopy, we demonstrate that the response of phosphatidylserine vesicles to adsorption of aSyn is strongly dependent on the acyl chain length. Incubation of aSyn with DOPS vesicles led rapidly to minor changes in vesicle shape from spherical to prolate ellipsoid. In contrast, aSyn dramatically remodeled DLPS vesicles into a diversity of discoids, tubules, ribbons, and sheets in a process that continued for hours. Simulations revealed that adsorption of aSyn to DLPS but not DOPS caused a marked elongation of vesicles, followed by preferential redistribution of the monomers to the highly curved polar regions of the elongated vesicles, resulting in high localized protein concentrations supportive of accelerated aggregation. We observed unusual morphologies of twisted and helical ribbons and sheets in mixtures of aSyn and DLPS well before fluorescence detection of amyloid aggregates. Our experimental and computational works challenge the prevailing hypothesis that acidic lipid vesicles nucleate aSyn aggregation by passively providing a surface for protein concentration. Our results point to a more complex story, in which aggregation requires *active* responses of aSyn and membrane to each other. Lipid compositions with lower bending rigidity might facilitate aSyn-mediated membrane remodeling as a part of aSyn's normal role in synaptic vesicle trafficking but may conversely also facilitate pathological aggregation via the concerted action of its curvature generating and sensing roles. These findings provide new insights into the mechanism by which aSyn-induced membrane remodeling, not simply membrane adsorption, drives lipid-bilayer stimulation of protein aggregation.

ASSOCIATED CONTENT

Supporting Information

The Supporting Information is available free of charge at https://pubs.acs.org/doi/10.1021/acs.jpcb.0c09192.

https://dx.doi.org/10.1021/acs.jpcb.0c09192
J. Phys. Chem. B 2021, 125, 1582−1594

Experimental methods; simulation methods; analysis of particle shapes; Figures S1−S17 and Tables S1−S4; references (PDF)

AUTHOR INFORMATION

Corresponding Author

Regina M. Murphy − *Department of Chemical and Biological Engineering, University of Wisconsin, Madison, Wisconsin 53706, United States;* orcid.org/0000-0002-6196-5450; Email: regina.murphy@wisc.edu

Authors

Brandon M. Hoover − *Biophysics Program, University of Wisconsin, Madison, Wisconsin 53706, United States*

Zhizhang Shen − *Department of Chemical and Biological Engineering, University of Wisconsin, Madison, Wisconsin 53706, United States*

Curran G. Gahan − *Department of Chemical and Biological Engineering, University of Wisconsin, Madison, Wisconsin 53706, United States*

David M. Lynn − *Department of Chemical and Biological Engineering, University of Wisconsin, Madison, Wisconsin 53706, United States*

Reid C. Van Lehn − *Biophysics Program and Department of Chemical and Biological Engineering, University of Wisconsin, Madison, Wisconsin 53706, United States;* orcid.org/0000-0003-4885-6599

Complete contact information is available at: https://pubs.acs.org/10.1021/acs.jpcb.0c09192

Author Contributions

B.M.H. prepared materials, performed fluorescence, NTA, and CD experiments, analyzed data, and wrote the manuscript. Z.S. developed and ran simulations and analyzed results. C.G.G. performed TEM experiments and analyzed results. D.M.L. designed experiments, analyzed results, and edited the manuscript. R.C.V. designed simulations, analyzed results, and wrote sections of the manuscript. R.M.M. designed experiments, coordinated work, analyzed results, and wrote and edited the manuscript.

Notes

The authors declare no competing financial interest.

ACKNOWLEDGMENTS

Funding for this work was provided by the National Science Foundation CBET-1703237 and the William F. Vilas Trust of the University of Wisconsin. Computational work used the Extreme Science and Engineering Discovery Environment (XSEDE), which is supported by National Science Foundation grant number ACI-1548562.

REFERENCES

(1) Rocca, W. A. The burden of Parkinson's disease: a worldwide perspective. *Lancet Neurol.* **2018**, *17*, 928−929.

(2) Ball, N.; Teo, W.-P.; Chandra, S.; Chapman, J. Parkinson's disease and the environment. *Front. Neurol.* **2019**, *10*, 218.

(3) Spillantini, M. G.; Schmidt, M. L.; Lee, V.M.-Y.; Trojanowski, J. Q.; Jakes, R.; Goedert, M. α-Synuclein in Lewy bodies. *Nature* **1997**, *388*, 839−840.

(4) Spillantini, M. G.; Crowther, R. A.; Jakes, R.; Hasegawa, M.; Goedert, M. Alpha-synuclein in filamentous inclusions of Lewy bodies from Parkinson's disease and dementia with lewy bodies. *Proc. Natl. Acad. Sci. U. S. A.* **1998**, *95*, 6469−6473.

(5) Shahmoradian, S. H.; Lewis, A. J.; Genoud, C.; Hench, J.; Moors, T. E.; Navarro, P. P.; Castaño-Díez, D.; Schweighauser, G.; Graff-Meyer, A.; Goldie, K. N.; et al. Lewy pathology in Parkinson's disease consists of crowded organelles and lipid membranes. *Nat. Neurosci.* **2019**, *22*, 1099−1109.

(6) Araki, K.; Yagi, N.; Aoyama, K.; Choong, C.-J.; Hayakawa, H.; Fujimura, H.; Nagai, Y.; Goto, Y.; Mochizuki, H. Parkinson's disease is a type of amyloidosis featuring accumulation of amyloid fibrils of α-synuclein. *Proc. Natl. Acad. Sci. U. S. A.* **2019**, *116*, 17963−17969.

(7) Uversky, V. N.; Li, J.; Souillac, P.; Millett, I. S.; Doniach, S.; Jakes, R.; Goedert, M.; Fink, A. L. Biophysical properties of the synucleins and their propensities to fibrillate: inhibition of α-synuclein assembly by β- and γ-synucleins. *J. Biol. Chem.* **2002**, *277*, 11970−11978.

(8) Buell, A. K.; Galvagnion, C.; Gaspar, R.; Sparr, E.; Vendruscolo, M.; Knowles, T. P. J.; Linse, S.; Dobson, C. M. Solution conditions determine the relative importance of nucleation and growth processes in α-synuclein aggregation. *Proc. Natl. Acad. Sci. U. S. A.* **2014**, *111*, 7671−7676.

(9) Uversky, V. N. A protein-chameleon: conformational plasticity of α-synuclein, a disordered protein involved in neurodegenerative disorders. *J. Biomol. Struct. Dyn.* **2003**, *21*, 211−234.

(10) Jo, E.; McLaurin, J.; Yip, C. M.; St. George-Hyslop, P.; Fraser, P. E. α-Synuclein membrane interactions and lipid specificity. *J. Biol. Chem.* **2000**, *275*, 34328−34334.

(11) Davidson, W. S.; Jonas, A.; Clayton, D. F.; George, J. M. Stabilization of α-synuclein secondary structure upon binding to synthetic membranes. *J. Biol. Chem.* **1998**, *273*, 9443−9449.

(12) Georgieva, E. R.; Ramlall, T. F.; Borbat, P. P.; Freed, J. H.; Eliezer, D. The lipid-binding domain of wild type and mutant α-synuclein: compactness and interconversion between the broken and extended helix forms. *J. Biol. Chem.* **2010**, *285*, 28261−28274.

(13) Shvadchak, V. V.; Falomir-Lockhart, L. J.; Yushchenko, D. A.; Jovin, T. M. Specificity and kinetics of α-synuclein binding to model membranes determined with fluorescent excited state intramolecular proton transfer (ESIPT) probe. *J. Biol. Chem.* **2011**, *286*, 13023−13032.

(14) Middleton, E. R.; Rhoades, E. Effects of curvature and composition on α-synuclein binding to lipid vesicles. *Biophys. J.* **2010**, *99*, 2279−2288.

(15) Galvagnion, C.; Brown, J. W. P.; Ouberai, M. M.; Flagmeier, P.; Vendruscolo, M.; Buell, E.; Sparr, A. K.; Dobson, C. M. hemical properties of lipids strongly affect the kinetics of the membrane-induced aggregation of α-synuclein. *Proc. Natl. Acad. Sci. U. S. A.* **2016**, *113*, 7065−7070.

(16) Nuscher, B.; Kamp, F.; Mehnert, F.; Odoy, F.; Haass, C.; Kahle, P. J.; Beyer, K. α-Synuclein has a high affinity for packing defects in a bilayer membrane: a thermodynamics study. *J. Biol. Chem.* **2004**, *279*, 21966−21975.

(17) Ouberai, M. M.; Wang, J.; Swann, M. J.; Galvagnion, C.; Guilliams, T.; Dobson, C. M.; Welland, M. E. α-Synuclein senses lipid packing defects and induces lateral expansion of lipids leading to membrane remodeling. *J. Biol. Chem.* **2013**, *288*, 20883−20895.

(18) Varkey, J.; Isas, J. M.; Mizuno, N.; Jensen, M. B.; Bhatia, V. K.; Jao, C. C.; Petrlova, J.; Voss, J. C.; Stamou, D. G.; Steven, A. C.; Langen, R. Membrane curvature induction and tubulation are common features of synucleins and apolipoproteins. *J. Biol. Chem.* **2010**, *285*, 32486−32493.

(19) O'Leary, E. I.; Lee, J. C. Interplay between α-synuclein amyloid formation and membrane structure. *Biochim. Biophys. Acta, Proteins Proteomics* **2019**, *1867*, 483−491.

(20) Westphal, C. H.; Chandra, S. S. Monomeric synucleins generate membrane curvature. *J. Biol. Chem.* **2013**, *288*, 1829−1840.

(21) Grey, M.; Linse, S.; Nilsson, H.; Brundin, P.; Sparr, E. Membrane interaction of α-synuclein in different aggregation states. *J. Parkinson's Dis.* **2011**, *1*, 359−371.

(22) Grey, M.; Dunning, C. J.; Gaspar, R.; Grey, C.; Brundin, P.; Sparr, E.; Linse, S. Acceleration of α-synuclein aggregation by exosomes. *J. Biol. Chem.* **2015**, *290*, 2969−2982.

(23) Gaspar, R.; Pallbo, J.; Weininger, U.; Linse, S.; Sparr, E. Ganglioside lipids accelerate α-synuclein amyloid formation. *Biochim. Biophys. Acta, Proteins Proteomics* **2018**, *1866*, 1062−1072.
(24) Galvagnion, C.; Buell, A. K.; Meisl, G.; Michaels, T. C. T.; Vendruscolo, M.; Knowles, T. P. J.; Dobson, C. M. Lipid vesicles trigger α-synuclein aggregation by stimulating primary nucleation. *Nat. Chem. Biol.* **2015**, *11*, 229−234.
(25) Zhu, M.; Li, J.; Fink, A. L. The association of α-synuclein with membranes affects bilayer structure, stability, and fibril formation. *J. Biol. Chem.* **2003**, *278*, 40186−40197.
(26) Mizuno, N.; Varkey, J.; Kegulian, N. C.; Hegde, B. G.; Cheng, N.; Langen, R.; Steven, A. C. Remodeling of lipid vesicles into cylindrical micelles by α-synuclein in an extended α-helical conformation. *J. Biol. Chem.* **2012**, *287*, 29301−29311.
(27) Jiang, Z.; Flynn, J. D.; Teague, W. E.; Gawrisch, K.; Lee, J. C. Stimulation of α-synuclein amyloid formation by phosphatidylglycerol micellar tubules. *Biochim. Biophys. Acta, Biomembr.* **2018**, *1860*, 1840−1847.
(28) Jiang, Z.; de Messieres, M.; Lee, J. C. Membrane remodeling by α-synuclein and effects on amyloid formation. *J. Am. Chem. Soc.* **2013**, *135*, 15970−15973.
(29) Hoover, B. M.; Murphy, R. M. Evaluation of nanoparticle tracking analysis for the detection of rod-shaped particles and protein aggregates. *J. Pharm. Sci.* **2020**, *109*, 452−463.
(30) Wu, Z.; Cui, Q.; Yethiraj, A. A new coarse-grained model for water: the importance of electrostatic interactions. *J. Phys. Chem. B* **2010**, *114*, 10524−10529.
(31) Wu, Z.; Cui, Q.; Yethiraj, A. A new coarse-grained force field for membrane-peptide simulations. *J. Chem. Theory Comput.* **2011**, *7*, 3793−3802.
(32) Ulmschneider, J. P.; Smith, J. C.; White, S. H.; Ulmschneider, M. B. In silico partitioning and transmembrane insertion of hydrophobic peptides under equilibrium conditions. *J. Am. Chem. Soc.* **2011**, *133*, 15487−15495.
(33) Noé, F.; Schütte, C.; Vanden-Eijnden, E.; Reich, L.; Weikl, T. R. Constructing the equilibrium ensemble of folding pathways from short off-equilibrium simulations. *Proc. Natl. Acad. Sci. U. S. A.* **2009**, *106*, 19011−19016.
(34) Chng, C.-P. Effect of simulation temperature on phospholipid bilayer-vesicle transition studied by coarse-grained molecular dynamics simulations. *Soft Matter* **2013**, *9*, 7294.
(35) Brandt, E. G.; Braun, A. R.; Sachs, J. N.; Nagle, J. F.; Edholm, O. Interpretation of fluctuation spectra in lipid bilayer simulations. *Biophys. J.* **2011**, *100*, 2104−2111.
(36) Pan, J.; Tristram-Nagle, S.; Kučerka, N.; Nagle, J. F. Temperature dependence of structure, bending rigidity, and bilayer interactions of dioleoylphosphatidylcholine bilayers. *Biophys. J.* **2008**, *94*, 117−124.
(37) Braun, A. R.; Lacy, M. M.; Ducas, V. C.; Rhoades, E.; Sachs, J. N. α-Synuclein-induced membrane remodeling is driven by binding affinity, partition depth, and interleaflet order asymmetry. *J. Am. Chem. Soc.* **2014**, *136*, 9962−9972.
(38) Braun, A. R.; Lacy, M. M.; Ducas, V. C.; Rhoades, E.; Sachs, J. N. α-Synuclein's uniquely long amphipathic helix enhances its membrane binding and remodeling capacity. *J. Membr. Biol.* **2017**, *250*, 183−193.
(39) Kim, H.-Y.; Huang, B. X.; Spector, A. A. Phosphatidylserine in the brain: Metabolism and function. *Prog. Lipid Res.* **2014**, *56*, 1−18.
(40) Almeida, P. F.; Pokorny, A. Mechanisms of antimicrobial, cytolytic, and cell-penetrating peptides: From kinetics to thermodynamics. *Biochemistry* **2009**, *48*, 8083−8093.
(41) Apellániz, B.; Nieva, J. L.; Schwille, P.; García-Sáez, A. J. All-or-none versus graded: Single-vesicle analysis reveals lipid composition effects on membrane permeabilization. *Biophys. J.* **2010**, *99*, 3619−3628.
(42) Filipe, V.; Hawe, A.; Jiskoot, W. Critical evaluation of nanoparticle tracking analysis (NTA) by nanosight for the measurement of nanoparticles and protein aggregates. *Pharm. Res.* **2010**, *27*, 796−810.
(43) Dragovic, R. A.; Gardiner, C.; Brooks, A. S.; Tannetta, A. S.; Ferguson, D. J. P.; Hole, P.; Carr, B.; Redman, C. W. G.; Harris, A. L.; Dobson, P. J.; et al. Sizing and phenotyping of cellular vesicles using nanoparticle tracking analysis. *Nanomedicine* **2011**, *7*, 780−788.
(44) Gang, H.; Galvagnion, C.; Meisl, G.; Müller, T.; Pfammatter, M.; Buell, A. K.; Levin, A.; Dobson, C. M.; Mu, B.; Knowles, T. P. J. Microfluidic diffusion platform for characterizing the sizes of lipid vesicles and the thermodynamics of protein-lipid interactions. *Anal. Chem.* **2018**, *90*, 3284−3290.
(45) Burré, J.; Sharma, M.; Südhof, T. C. α-Synuclein assembles into higher-order multimers upon membrane binding to promote SNARE complex formation. *Proc. Natl. Acad. Sci. U. S. A.* **2014**, *111*, E4274−E4283.
(46) Jao, C. C.; Hegde, B. G.; Chen, J.; Haworth, I. S.; Langen, R. Structure of membrane-bound -synuclein from site-directed spin labeling and computational refinement. *Proc. Natl. Acad. Sci. U. S. A.* **2008**, *105*, 19666−19671.
(47) Pfefferkorn, C. M.; Jiang, Z.; Lee, J. C. Biophysics of α-synuclein membrane interactions. *Biochim. Biophys. Acta, Biomembr.* **2012**, *1818*, 162−171.
(48) Nelson, D. L.; Cox, M. M.; Hoskins, A. A. *Lehninger: Principles of Biochemistry*, 8th ed.; W.H. Freeman: New York, 2021.
(49) Dikiy, I.; Eliezer, D. Folding and misfolding of alpha-synuclein on membranes. *Biochim. Biophys. Acta, Biomembr.* **2012**, *1818*, 1013−1018.
(50) Yang, D. T.; Lu, X.; Fan, Y.; Murphy, R. M. Evaluation of nanoparticle tracking for characterization of fibrillar protein aggregates. *AIChE J.* **2014**, *60*, 1236−1244.
(51) Murphy, R. M.; Lee, C. C. In *Misbehaving Proteins: Protein (Mis)folding, Aggregation, and Stability*; Murphy, R. M., Tsai, A. M., Eds.; Springer: New York, 2006; pp 147−165.
(52) Zhao, H.; Brown, P. H.; Schuck, P. On the distribution of protein refractive index increments. *Biophys. J.* **2011**, *100*, 2309−2317 2011.
(53) Theisen, A. *Refractive Increment Data-Book for Polymer and Biomolecular Scientists*; Nottingham University Press: Nottingham, UK, 2000.
(54) Mathai, J. C.; Tristram-Nagle, S.; Nagle, J. F.; Zeidel, M. L. Structural determinants of water permeability through the lipid membrane. *J. Gen. Physiol.* **2008**, *131*, 69−76.
(55) Wu, Z.; Cui, Q.; Yethiraj, A. Why do arginine and lysine organize lipids differently? Insights from coarse-grained and atomistic simulations. *J. Phys. Chem. B* **2013**, *117*, 12145−12156.
(56) Sheavly, J. K.; Pedersen, J. A.; Van Lehn, R. C. Curvature-driven adsorption of cationic nanoparticles to phase boundaries in multicomponent lipid bilayers. *Nanoscale* **2019**, *11*, 2767−2778.
(57) Das, M.; Dahal, U.; Mesele, O.; Liang, D.; Cui, Q. Molecular dynamics simulation of interaction between functionalized nanoparticles with lipid membranes: Analysis of coarse-grained models. *J. Phys. Chem. B* **2019**, *123*, 10547−10561.
(58) Caparotta, M.; Bustos, D. M.; Masone, D. Order-disorder skewness in alpha-synuclein: a key mechanism to recognize membrane curvature. *Phys. Chem. Chem. Phys.* **2020**, *22*, 5255−5263.
(59) Greenfield, N. J. Using circular dichroism spectra to estimate protein secondary structure. *Nat. Protoc.* **2006**, *1*, 2876−2890.
(60) West, A.; Brummel, B. E.; Braun, A. R.; Rhoades, E.; Sachs, J. N. Membrane remodeling and mechanics: Experiments and simulations of α-synuclein. *Biochim. Biophys. Acta, Biomembr.* **2016**, *1858*, 1594−1609.
(61) Simunovic, M.; Srivastava, A.; Voth, G. A. Linear aggregation of proteins on the membrane as a prelude to membrane remodeling. *Proc. Natl. Acad. Sci. U. S. A.* **2013**, *110*, 20396−20401.
(62) Dehsorkhi, A.; Castelletto, V.; Hamley, I. W. Self-assembling amphiphilic peptides. *J. Pept. Sci.* **2014**, *20*, 453−467.
(63) Adamcik, J.; Mezzenga, R. Amyloid polymorphism in the protein folding and aggregation energy landscape. *Angew. Chem., Int. Ed.* **2018**, *57*, 8370−8382.
(64) Reynolds, N. P.; Adamcik, J.; Berryman, J. T.; Handschin, S.; Zanjani, A. A. H.; Li, W.; Liu, K.; Zhang, A.; Mezzenga, R.

Competition between crystal and fibril formation in molecular mutations of amyloidogenic peptides. *Nat. Commun.* **2017**, *8*, 1338.
(65) Morris, K. L.; Zibaee, S.; Chen, L.; Goedert, M.; Sikorski, P.; Serpell, L. C. The structure of cross-β tapes and tubes formed by an octapeptide, $\alpha S\beta 1$. *Angew. Chem., Int. Ed.* **2013**, *52*, 2279−2283.
(66) Galvagnion, C.; Topgaard, D.; Makasewicz, K.; Buell, A. K.; Linse, S.; Sparr, E.; Dobson, C. M. Lipid dynamics and phase transition within α-synuclein amyloid fibrils. *J. Phys. Chem. Lett.* **2019**, *10*, 7872−7877.
(67) Viennet, T.; Wördehoff, M. M.; Uluca, B.; Poojari, C.; Shaykhalishahi, H.; Willbold, D.; Strodel, B.; Heise, H.; Buell, A. K.; Hoyer, W.; Etzkorn, M. Structural insights from lipid-bilayer nanodiscs link α-synuclein membrane-binding modes to amyloid fibril formation. *Commun. Biol.* **2018**, *1*, 44.
(68) Campioni, S.; Carret, G.; Jordens, S.; Nicoud, L.; Mezzenga, R.; Riek, R. The presence of an air-water interface affects formation and elongation of α-synuclein fibrils. *J. Am. Chem. Soc.* **2014**, *136*, 2866−2875.
(69) Kiskis, J.; Horvath, I.; Wittung-Stafshede, P.; Rocha, S. Unraveling amyloid formation paths of Parkinson's disease protein α-synuclein triggered by anionic vesicles. *Q. Rev. Biophys.* **2017**, *50*, No. e3.

https://dx.doi.org/10.1021/acs.jpcb.0c09192
J. Phys. Chem. B 2021, 125, 1582−1594